A chemically soldered polyoxometalate single-molecule transistor†

Chuanli Wu, Xiaohang Qiao, Craig M. Robertson, Simon J. Higgins, Chenxin Cai, Richard J. Nichols and Andrea Vezzoli*

† Ms. Chuanli Wu, Ms. Xiaohang Qiao, Dr. Craig M. Robertson, Prof. Simon J. Higgins, Prof. Richard J. Nichols and Dr. Andrea Vezzoli
Department of Chemistry, University of Liverpool, Crown Street, Liverpool L69 7ZD, United Kingdom
e-mail for Dr. Andrea Vezzoli: andrea.vezzoli@liverpool.ac.uk

Ms. Chuanli Wu and Prof. Chenxin Cai
School of Chemistry and Materials Science, Nanjing Normal University, Nanjing 210023, People's Republic of China

Dr. Andrea Vezzoli
Stephenson Institute for Renewable Energy, University of Liverpool, Peach Street, Liverpool L69 7ZF, United Kingdom

* corresponding author

Abstract

Polyoxometalates have been proposed in the literature as promising components for nanoelectronic applications, where they could offer key advantages with their structural versatility and rich electrochemistry. Apart from a few studies on their ensemble behaviour (for instance, as monolayers or thin films) this potential remains largely unexplored. We synthesised a pyridyl-capped Anderson-Evans polyoxometalate and used it to fabricate single-molecule junctions, by using the organic termini to chemically "solder" a single metal oxide cluster to two nanoelectrodes through coordination bonds. Operating the device in an electrochemical environment allowed us to probe charge transport through different oxidation states of the polyoxometalate, and we report here an efficient three-state transistor behaviour. Conductance data fits a quantum tunnelling transport mechanism, with charge having different tunnelling probabilities through different oxidation states of the polyoxometalate. Our results show the promise of such compounds in nanoelectronics, and are, to our best knowledge, the first report on the single-entity electrochemical behaviour of polyoxometalates.

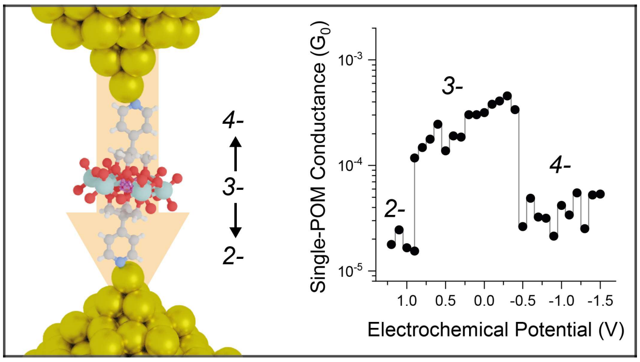

Main Text

Assemblies of molecules, or even single molecules, might in the future offer new approaches to traditional nanoelectronics and nanofabrication, and contribute to scalability with a bottom-up self-assembly approach and miniaturisation.[1] A key aspect of molecular electronics from a chemists' perspective is however the possibility of exploring a large chemical space to (i) tune the device response to the desired range and magnitude, obtaining in turn important insights on structure-properties relationships and (ii) study phenomena unique to the molecular and quantum world. Since the first pioneering studies in the late 1990s,[2] single-molecule devices with behaviour like semiconductor-based diodes,[3,4] resistors,[5] switches[6–9] and transistors[10–13] have been demonstrated, and the chemical complexity of the molecules used to fabricate junctions has rapidly increased. Stemming from the original studies employing simple aliphatic and conjugated, rod-like, oligoaryl moieties,[14] it is now common to read reports on molecular wires incorporating fused polyaromatic/heterocyclic systems,[15,16] supramolecular complexes,[17,18] organometallic centres[19,20] and, more recently, polynuclear clusters.[21–24] The latter are particularly interesting from a technology point of view for their electronic behaviour, as the presence of multiple metallic centres imparts stability to several oxidation states, with the cluster accommodating large charge variations. These electron-sink phenomena[25] (*i.e.* clusters are able to accept and release electrons reversibly without significant changes in their structure) resulted in great interest in their synthesis and applications, especially as electroactive materials to be deployed in electronic, sensing and catalytic devices.[26,27]

Polyoxometalates (POMs) are a class of cluster compounds noteworthy for their stability and rich electrochemistry.[28] The relatively high oxidation state of the metallic centres linked together by μ_2-oxido ligands gives them less susceptibility to decomposition both in ambient atmosphere and in solution, resulting in stability over multiple redox states. In recent years, much effort has been devoted to the functionalisation of POMs with organic moieties,[29] to impart properties such as biocompatibility[30] and luminescence,[31,32] and to provide additional metal-binding sites for the synthesis of coordination polymers and three-dimensional frameworks.[33] Metallophilic termini can however be also exploited in molecular electronics as electrode anchoring groups,[34,35] to ensure clear junction formation and provide a strong mechanical stability and high electronic coupling between the molecule and the source/drain electrodes. While perspectives on the promise of polyoxometalates as molecular electronic components have indeed been featured in publications,[36,37] experimental reports are limited to a few niche studies, mostly on their behaviour as a nanoscale ensemble (*i.e.* a monolayer or a thin film)[22,38,39] or immobilised on a metal surface.[40] We therefore focussed on the synthesis of the Anderson-Evans cluster (Figure 1a and 1b) functionalised with pyridyl ligands **1,** (NC_5H_4)-C-$(CH_2O)_3$≡$[MnMo_6O_{18}]$≡$(OCH_2)_3$-C-(C_5H_4N), to then use it as molecular wire for the fabrication of chemically soldered[21] single-polyoxometalate junctions. In this contribution, we explore its single-entity electrochemistry, and we find a remarkable three-state transistor behaviour, with both ON/OFF ratios exceeding one order of magnitude.

Results and Discussion

We followed a published procedure[33] for the synthesis of compound **1** (more details in the SI) as a tris(tetrabutylammonium) salt. To confirm the structure of the polyoxometalate, we grew crystals by vapour diffusion of diethyl ether into a concentrated solution of **1** in dimethylformamide and obtained samples suitable for XRD (Figure 1a-b).

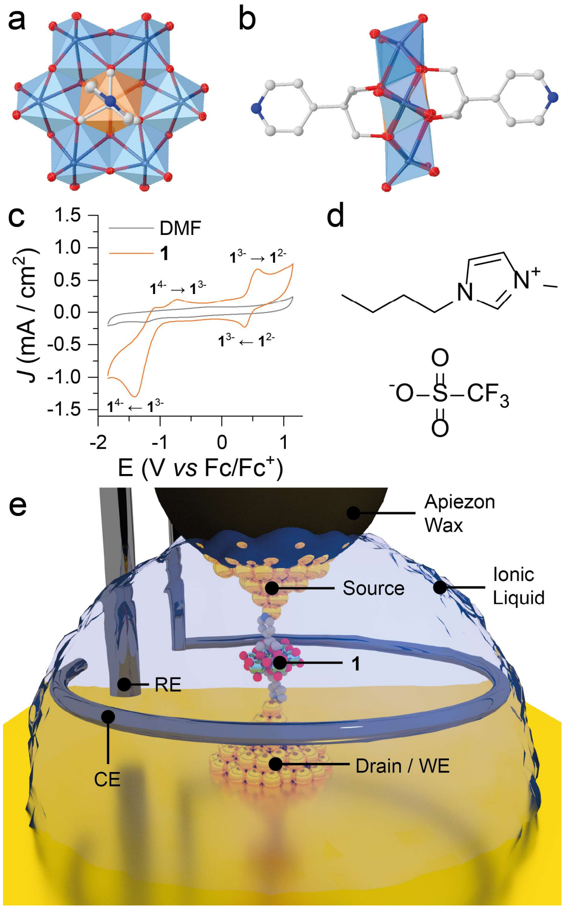

Figure 1: Details on the experiments presented in this study: a) top view of **1** (SCXRD structure). b) Side view of **1** (SCXRD structure). See SI for more details on the structure of **1**. c) Cyclic voltammetry of **1** (10 mM) in in DMF with 0.1 M NBu_4BF_4 as support electrolyte, using a glassy carbon working electrode, Pt wire counter electrode and Pt wire quasi reference electrode. Ferrocene was added at the end of the experiment as a standard (see SI for calibration and additional data). Scan speed 100 mV/s d) Structure of the ionic liquid BMIM-OTf used in this study. e) Depiction of the single-POM junction in the 4-electrode configuration controlled by the bipotentiostat. WE = working electrode; CE = counter electrode; RE = reference electrode. Legend for panels (a) and (b): teal polyhedra: $\{MoO_6\}$; orange polyhedra: $\{MnMo_6\}$; grey spheres: C; blue spheres: N; red ellipsoids: O. H atoms and counterions (3 x NBu_4^+) not shown for clarity.

The compound itself showed an interesting electrochemical behaviour at a glassy carbon electrode. Two quasi-reversible redox couples can be observed, and these have been related to the reduction and oxidation of the central Mn atom ($Mn^{III} \rightleftarrows Mn^{II}$ and $Mn^{III} \rightleftarrows Mn^{IV}$), a behaviour already found in amine- and TTF-capped analogues.[41] For the pyridyl-capped POM **1**, the reduction process is very clearly electrochemically irreversible, with a peak-to-peak separation of ~600 mV at low scan rates. The oxidation process is less irreversible, with a reduced peak-to-peak separation of ~180 mV (see SI for more details).

We then fabricated junctions using the scanning tunnelling microscopy break junction (*STM-BJ*) method,[42] by driving a Au tip towards a Au substrate under constant DC bias until it crashes and forms a metallic contact having conductance $> 5G_0$ (G_0 = conductance quantum, $2e^2/h \cong 77.48\ \mu S$). The tip is then withdrawn at constant speed, and the metallic contact is thinned down to a single atom (having conductance $= G_0$) and then broken. When the experiment is performed in a solution of a molecular wire having metal-binding moieties at its termini, molecular junctions self-assemble in the freshly formed nanogap. The process is repeated thousands of times while recording the current, and the conductance of the junctions is then calculated as $G = I/V_{BIAS}$. The traces obtained in the process (as current *vs* electrode position) are then analysed statistically as histograms and density maps, to calculate the most probable conductance value. The experiments were performed under electrochemical control, using a bipotentiostat and a 4-electrode cell, with the Au substrate as working electrode, a platinum counter electrode and a platinum reference electrode (Figure 1e). This setup was found to have an open circuit potential of -0.23 V vs Fc/Fc^+. The STM tip was coated with Apiezon wax[43] to reduce faradaic currents, and constantly biased against the working electrode (V_{BIAS} = 200 mV in this study) by the bipotentiostat, to ensure the two Au electrodes act as source and drain. The measurements were performed with the four electrodes immersed in the ionic liquid BMIM-OTf (Figure 1c) with a 1 mM concentration of compound **1**. The use of ionic liquids ensures a high degree of molecule-gate coupling[10] and they are an ideal medium for STM experiments and measurements, with low faradaic current attainable with insulated tips and a wide electrochemical window.[44–46] More details about the *STM-BJ* experiments, the electrochemistry of **1** in ionic liquid and the equipment used in this study can be found in the methods section and in the SI.

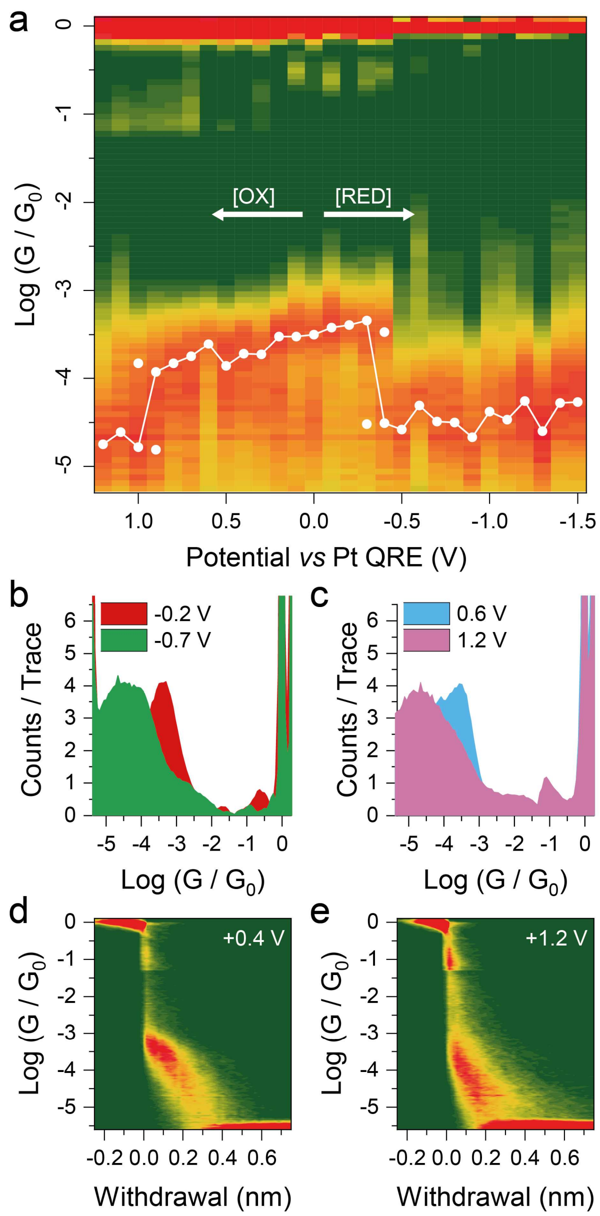

Figure 2: Single-molecule electrochemical gating experiments on **1**. a) heatmap of conductance across the electrochemical window explored, with overlaid in white the gaussian fitting of the conductance peaks (error bars = $\pm 1/2$ FWHM). Double points are shown in the vicinity of the switching potential. b) Conductance histograms for compound **1** at -0.2 V and -0.7 V electrochemical potential. c) Conductance histogram of **1** at 0.6 V and 1.2 V potential. d) 2D conductance *vs* electrode separation density map at 0.4 V potential. e) 2D conductance *vs* electrode separation density map at 1.2 V potential. Heatmap in (a) compiled with 10 bins per conductance decade. Conductance histograms in (b) and (c) compiled with 20 bins per conductance decade. 2D density maps in (d) and (e) compiled with 100 bins per conductance decade and 50 bins per nanometre. More than 3500 individual breaking traces have been collected at each potential. In all heatmaps and density plots green = low counts and red = high counts. More experimental results are presented in the SI.

The main results are shown in Figure 2. We explored the bias window between 1.2 V and -1.5 V vs Pt, which is attainable in the ionic liquid we used and where **1** exhibited three distinct charge states. As can be observed in Figure 2a, when the electrochemical potential is moved from zero towards more negative values, there is a slight increase in conductance as the potential acts as an electrostatic gate and moves the Fermi level towards a transport resonance. However, when the potential reaches -0.3 V vs Pt, the cluster accepts an electron and its charge state switches[41,47] to -4, with a strong effect on the conductance that drops by more than one order of magnitude, from $10^{-3.4}$ G_0 to $10^{-4.6}$ G_0. Close to the equilibrium potential, both charge states are present, and they almost equally contribute to the conductance histogram (see all histograms in the SI and later in the manuscript for the analysis). As the potential is made more negative, the electrostatic gate effect is reinstated, and conductance gradually climbs to $10^{-4.3}$ G_0. On the other hand, as the potential is made more positive from zero, the conductance is gradually reduced due to the electrostatic gate effect, until the charge state of the POM switches to -2, and its value falls to almost 10^{-5} G_0.

Two main things can be inferred from the above results. First, the observed electrostatic gate effect, where conductance increases as the potential is made more negative, strongly suggests that charge transport happens through a non-resonant, one-step tunnelling mechanism, assisted by the molecular LUMO (pyridyls are known[35] to promote LUMO-based conductance). Second, that the oxidation and reduction of the central Mn atom have a profound effect on the electronic structure of the POM, as the conductance is electrochemically gated by approximately an order of magnitude in both cases. The confirmation of a tunnelling mechanism, and the clear absence of a bell-shaped conductance enhancement at the equilibrium potential, discount a possible interpretation based on a two-step Kuznetsov-Ulstrup process (a hopping-type model associated with a conductance increase near the redox potential).[48,49] A Nernstian model based on charge tunnelling through different redox states of a molecule (in thermodynamic equilibrium depending on the applied electrochemical potential) has been developed to aid the interpretation of data obtained from junctions based on electroactive ferrocenes[50] or anthraquinone-substituted DNA.[51] In this model, charge is transported by non-resonant tunnelling through either the oxidised or the reduced state of the molecule, and the average conductance of the junction is given by the equation:

$$\bar{G} = G_1 + \frac{1}{1 + exp\left[{}^{e}/_{k_B T}\,(E - E_0)\right]}(G_1 - G_2) \qquad \text{Eq. 1}$$

Where G_1 and G_2 are, respectively, the conductance of the molecular junction in the higher and lower oxidation states, e is the electron charge, k_B is the Boltzmann constant, T is the temperature, E is the electrochemical potential and $E_0$is the equilibrium potential. We calculated $\bar{G}$ as weighted arithmetic mean of the conductance histograms Gaussian fitting:

$$\bar{G} = \frac{G_1A_1 + G_2A_2}{A_1 + A_2} \qquad \text{Eq. 2}$$

using the peak centre as the value for G and the area under the Gaussian curve as A, after removal of the background tunnelling signal obtained from a control experiment performed in the pure, anhydrous solvent. The weighted average of the experimental points and the Nernstian model are in good agreement, as can be observed in in Figure 3. It is worth stressing that the Nernstian model is not a fitting to the experimental conductance values, as no variable was parameterised. The agreement between Eq. 1 and the empirical data thereby confirms non-resonant tunnelling as the dominant charge transport mechanism, with the molecule either reduced or oxidised in the junction, depending on the potential.

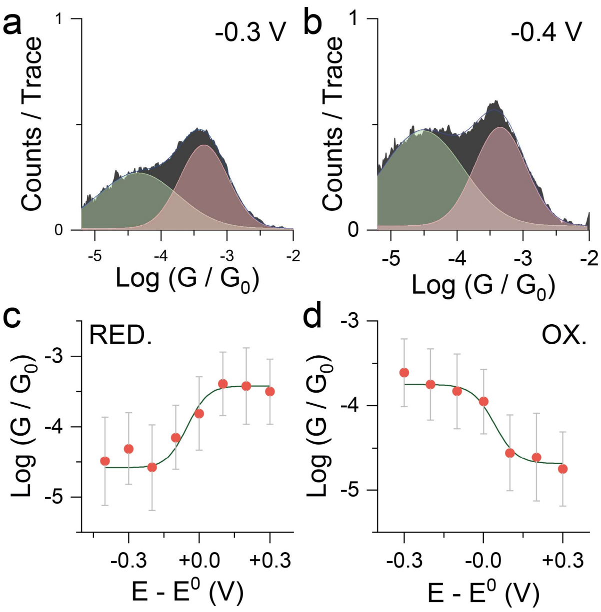

Figure 3: Gaussian fitting and Nernstian model. Examples of gaussian fitting of conductance histograms of **1** at an electrochemical potential of (a) -0.3 V and (b) -0.4 V, with the background tunnelling signal subtracted, used for the calculations of G_n and S_n. Further details on the background subtraction process are available in the SI. c) Average conductance (orange dots) vs equilibrium potential for the reduction process (E_0 = -0.3 V vs Pt). d) Average conductance (orange dots) vs equilibrium potential for the oxidation process (E_0 = 0.9 V vs Pt). The grey line in (c) and (d) is the Nernstian model obtained from Eq. 1. Histograms in (a) and (b) compiled with 100 bins per decade.

To further test the robustness of the junctions fabricated with the polyoxometalate **1**, we performed voltage ramps on stabilised junctions, in a 2-terminal device configuration. In this technique, a staircase ramp is applied to the piezo controlling the tip position, so that a specific position is held for 100 ms.

The height of the staircase (1 nm) was chosen to ensure the formation of a gap of size commensurate with the molecular length. During the hold portion of the ramp, the bias voltage is kept at a fixed value (100 mV) for 25 ms, then ramped to obtain an I/V characteristics or a high-voltage test, and then kept again at the fixed value for the final 25 ms (Figure 4a). Data is then sliced and processed using the automated algorithms described in the SI, to produce the 2d density maps presented in Figure 4. The I/V characteristics show a good ohmic behaviour up to relatively high biases (~ 0.7 V, see SI for linear scale plots) with no evident asymmetry or rectifying behaviour, further confirming an off-resonant tunnelling mechanism that also accounts for the observed relatively low conductance. As a stress test, we drove the junctions to biases higher than the one used to obtain the I/V behaviour, and we found excellent robustness under positive substrate bias, with the fabricated junctions surviving voltages up to 1.5 V.

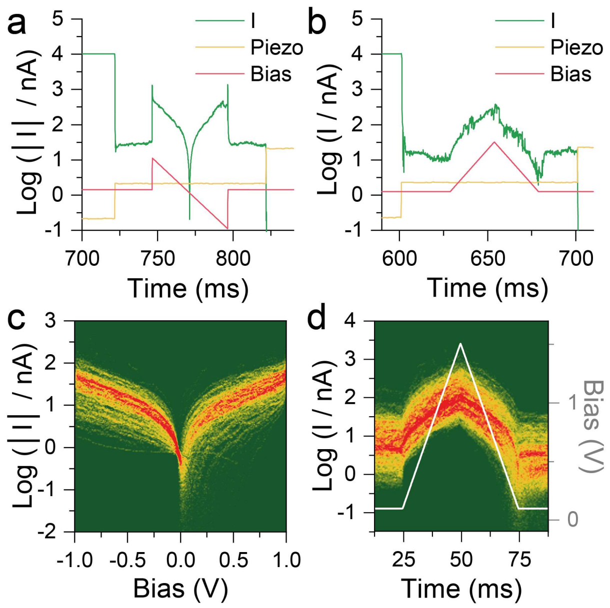

Figure 4: Two-terminal bias modulation experiments. Example (a) raw I/V data (-1 to 1 V sweep) and (b) raw high bias ramp curve (0.1 to 1.5 to 0.1 V sweep), with piezo and bias signal superimposed. c) 2d density map of the I/V characteristics for compound **1**, compiled from 1049 traces. d) 2d density map of current *vs* time during the high voltage ramp (superimposed in light grey), compiled from 922 traces. 2d maps in (c) and (d) compiled with 100 bins per current decade, 200 bins per volt and 2000 bins per second.

Conclusions

In conclusion, we have demonstrated here the use of a functionalised Anderson-Evans polyoxometalate in a three-state electrochemical transistor single-molecule device. The $MnMo_6O_{24}$ oxide cluster core is capped with two 4-pyridyl moieties that act as contact to the electrodes, allowing the fabrication of single-POM junctions. The junctions showed a clear OFF-ON-OFF behaviour under electrochemical control, with a difference in conductance of more than one order of magnitude between two adjacent charge states. The transistor-like behaviour arises from the POM being in three distinct charge states (-2, -3 and -4) depending on the applied electrochemical potential, and a clear electrostatic gating is further visible in the conductance *vs* potential plot. The results can be modelled within the framework of non-resonant tunnelling, with the charge states having a different tunnelling probability depending on the charge state of the molecular wire. The fabricated junctions are robust even under high bias, further showing the promise that POMs have in the field of molecular electronics, thanks to their multiple charge/oxidation states and high stability, and our results pave the way to a further use of such compounds in cluster electronics.

Methods

Compound **1** was prepared following a published procedure.[33] Junctions were fabricated using the *STM-BJ* technique,[42] using a modified Keysight 5500 electrochemical STM. Measurements were performed in 1 mM solutions of **1** in the ionic liquid 1-butyl-3-methylimidazolium trifluoromethanesulfonate (BMIM-OTf, IoLiTec GmbH). The ionic liquid was dehydrated by heating for >16 hours at 120 °C overnight *in vacuo* (~ 8 mbar) in the presence of 4Å molecular sieves. Measurements were performed using an Au tip (99.99+%, Goodfellow Cambridge Ltd) insulated with wax (Apiezon Wax W40, M&I Materials Ltd). Substrates were prepared by thermal evaporation of Au (99.99+%, Goodfellow Cambridge Ltd) on freshly cleaved muscovite mica (Agar Scientific Ltd). Conductance histograms were compiled with no data selection using >3500 consecutively measured traces. Cyclic voltammetry was performed with a Metrohm Autolab PGSTAT 128N potentiostat, in a standard three electrode configuration.

Further details on the synthesis of **1** (including spectroscopic and crystallographic data), the instrumentation used, and the data collection and analysis processes can be found in the SI.

Supporting Information:

Supporting information are available on the publisher website:

- Synthetic procedures and characterisation.
- Details on the *STM-BJ* experiments.

- Additional *STM-BJ* data.
- Additional details on the electrochemistry measurements.
- Crystal data.

Data Availability

The raw experimental *STM-BJ* data under electrochemical control, the processed data and the Python code used for its analysis can be found on the University of Liverpool data repository at DOI: 10.17638/datacat.liverpool.ac.uk/962. The raw experimental *STM-BJ* data used to compile the I/V characteristics and high bias behaviour, and the Labview code used for its analysis can be found on the University of Liverpool data repository at DOI: 10.17638/datacat.liverpool.ac.uk/967.

The SCXRD data is deposited on the Cambridge Crystallographic Dara Centre (deposition #1979403)

Acknowledgements

The authors thank D. Bethell for useful discussion on the Nernstian model and its interpretation. C.W. acknowledges funding from the China Scholarship Council (grant no. 201806860023). A.V. acknowledges funding from the Royal Society (University Research Fellowship URF\R1\191241) and the School of Physical Sciences of the University of Liverpool (Early Career Researchers & Returners Fund 2018). This work was further supported by UK EPSRC (grants EP/M005046/1, EP/M029522/1 and EP/M014169/1).

Author Contributions

A.V. conceived the project, and led it with the assistance of R.J.N. C.W. performed the *STM-BJ* and electrochemical measurements, assisted by X.Q. and A.V. Compound **1** was synthesised by A.V., and SCXRD data acquisition and analysis was performed by C.M.R. Data was analysed and interpreted by C.W., A.V., R.J.N. and S.J.H. The paper was written by A.V. with contributions from all the other authors.

Conflict of Interest

The authors declare no conflict of interest.

References

1. Ratner, M. A. A brief history of molecular electronics. *Nat. Nanotechnol.* **8**, 378–81 (2013).

2. Reed, M. A., Zhou, C., Muller, C. J., Burgin, T. P. & Tour, J. M. Conductance of a Molecular Junction. *Science (80-.).* **278**, 252–254 (1997).

3. Perrin, M. L. *et al.* A gate-tunable single-molecule diode. *Nanoscale* **8**, 8919–8923 (2016).

4. Capozzi, B. *et al.* Single-molecule diodes with high rectification ratios through environmental control. *Nat. Nanotechnol.* **10**, 522–527 (2015).

5. Garner, M. H. *et al.* Comprehensive suppression of single-molecule conductance using destructive σ-interference. *Nature* **558**, 415–419 (2018).

6. Ismael, A. K. *et al.* Side-Group-Mediated Mechanical Conductance Switching in Molecular Junctions. *Angew. Chemie Int. Ed.* **56**, 15378–15382 (2017).

7. Quek, S. Y. *et al.* Mechanically controlled binary conductance switching of a single-molecule junction. *Nat. Nanotechnol.* **4**, 230–234 (2009).

8. Liu, Z., Ren, S. & Guo, X. Switching Effects in Molecular Electronic Devices. *Top. Curr. Chem.* **375**, 1–33 (2017).

9. Taherinia, D. & Frisbie, C. D. Photoswitchable Hopping Transport in Molecular Wires 4 nm in Length. *J. Phys. Chem. C* **120**, 6442–6449 (2016).

10. Osorio, H. M. *et al.* Electrochemical Single-Molecule Transistors with Optimized Gate Coupling. *J. Am. Chem. Soc.* **137**, 14319–14328 (2015).

11. Brooke, R. J. *et al.* Single-Molecule Electrochemical Transistor Utilizing a Nickel-Pyridyl Spinterface. *Nano Lett.* **15**, 275–280 (2015).

12. Hosseini, S. *et al.* Single-Molecule Charge Transport and Electrochemical Gating in Redox-Active Perylene Diimide Junctions. *J. Phys. Chem. C* **120**, 22646–22654 (2016).

13. Darwish, N. *et al.* Observation of Electrochemically Controlled Quantum Interference in a Single Anthraquinone-Based Norbornylogous Bridge Molecule. *Angew. Chemie Int. Ed.* **51**, 3203–3206 (2012).

14. Wold, D. J., Haag, R., Rampi, M. A. & Frisbie, C. D. Distance Dependence of Electron Tunneling through Self-Assembled Monolayers Measured by Conducting Probe Atomic Force Microscopy: Unsaturated versus Saturated Molecular Junctions. *J. Phys. Chem. B* **106**, 2813–2816 (2002).

15. Cai, Z. *et al.* Exceptional Single-Molecule Transport Properties of Ladder-Type Heteroacene Molecular Wires. *J. Am. Chem. Soc.* **138**, 10630–10635 (2016).

16. Leary, E. *et al.* Bias-Driven Conductance Increase with Length in Porphyrin Tapes. *J. Am. Chem.*

Soc. **140**, 12877–12883 (2018).

17. Wang, K. *et al.* Charge transfer complexation boosts molecular conductance through Fermi level pinning. *Chem. Sci.* **10**, 2396–2403 (2019).

18. Zhang, W. *et al.* Single-Molecule Conductance of Viologen-Cucurbit[8]uril Host-Guest Complexes. *ACS Nano* **10**, 5212–5220 (2016).

19. Davidson, R. *et al.* Synthesis, Electrochemistry, and Single-Molecule Conductance of Bimetallic 2,3,5,6-Tetra(pyridine-2-yl)pyrazine-Based Complexes. *Inorg. Chem.* **54**, 5487–5494 (2015).

20. Tanaka, Y. *et al.* “Doping” of Polyyne with an Organometallic Fragment Leads to Highly Conductive Metallapolyyne Molecular Wire. *J. Am. Chem. Soc.* **140**, 10080–10084 (2018).

21. Roy, X. *et al.* Quantum soldering of individual quantum dots. *Angew. Chemie - Int. Ed.* **51**, 12473–12476 (2012).

22. de Bruijckere, J. *et al.* Ground-State Spin Blockade in a Single-Molecule Junction. *Phys. Rev. Lett.* **122**, 197701 (2019).

23. Tang, C. *et al.* Multicenter-Bond-Based Quantum Interference in Charge Transport Through Single-Molecule Carborane Junctions. *Angew. Chemie Int. Ed.* **58**, 10601–10605 (2019).

24. Ting, T. C. *et al.* Energy-Level Alignment for Single-Molecule Conductance of Extended Metal-Atom Chains. *Angew. Chemie - Int. Ed.* **54**, 15734–15738 (2015).

25. Fabrizi De Biani, F. *et al.* Redox Behavior of [H(6)(-)(n)()Ni(38)Pt(6)(CO)(48)](n)()(-) (n = 4-6) Anions: A Series of Metal Carbonyl Clusters Displaying Electron-Sink Features. *Inorg. Chem.* **38**, 3721–3724 (1999).

26. Mathew, A. & Pradeep, T. Noble metal clusters: Applications in energy, environment, and biology. *Part. Part. Syst. Charact.* **31**, 1017–1053 (2014).

27. Stuckart, M. & Monakhov, K. Y. Polyoxometalates as components of supramolecular assemblies. *Chem. Sci.* **10**, 4364–4376 (2019).

28. Sadakane, M. & Steckhan, E. Electrochemical Properties of Polyoxometalates as Electrocatalysts. *Chem. Rev.* **98**, 219–238 (1998).

29. Miras, H. N., Yan, J., Long, D. L. & Cronin, L. Engineering polyoxometalates with emergent properties. *Chem. Soc. Rev.* **41**, 7403–7430 (2012).

30. Blazevic, A. & Rompel, A. The Anderson–Evans polyoxometalate: From inorganic building blocks via hybrid organic–inorganic structures to tomorrows “Bio-POM”. *Coord. Chem. Rev.* **307**, 42–64 (2016).

31. Salomon, W. *et al.* A Multifunctional Dual-Luminescent Polyoxometalate@Metal-Organic Framework EuW10@UiO-67 Composite as Chemical Probe and Temperature Sensor. *Front.*

Chem. **6**, 1–8 (2018).

32. Bolle, P. *et al.* Strong Solid-state Luminescence Enhancement in Supramolecular Assemblies of Polyoxometalate and “Aggregation-Induced Emission”-active Phospholium. *Chem. - An Asian J.* **14**, 1642–1646 (2019).

33. Yazigi, F. J., Wilson, C., Long, D. L. & Forgan, R. S. Synthetic Considerations in the Self-Assembly of Coordination Polymers of Pyridine-Functionalized Hybrid Mn-Anderson Polyoxometalates. *Cryst. Growth Des.* **17**, 4739–4748 (2017).

34. Hihath, J. & Tao, N. J. The role of molecule–electrode contact in single-molecule electronics. *Semicond. Sci. Technol.* **29**, 054007 (2014).

35. Leary, E. *et al.* Incorporating single molecules into electrical circuits. The role of the chemical anchoring group. *Chem. Soc. Rev.* **44**, 920–942 (2015).

36. Monakhov, K. Y., Moors, M. & Kögerler, P. Perspectives for Polyoxometalates in Single-Molecule Electronics and Spintronics. *Adv. Inorg. Chem.* **69**, 251–286 (2017).

37. Vilà-Nadal, L. *et al.* Towards polyoxometalate-cluster-based nano-electronics. *Chem. - A Eur. J.* **19**, 16502–16511 (2013).

38. Sherif, S. *et al.* Current rectification in a single molecule diode: the role of electrode coupling. *Nanotechnology* **26**, 291001 (2015).

39. Laurans, M. *et al.* Molecular signature of polyoxometalates in electron transport of silicon-based molecular junctions. *Nanoscale* **10**, 17156–17165 (2018).

40. Linnenberg, O. *et al.* Addressing Multiple Resistive States of Polyoxovanadates: Conductivity as a Function of Individual Molecular Redox States. *J. Am. Chem. Soc.* **140**, 16635–16640 (2018).

41. Boulmier, A. *et al.* Anderson-type polyoxometalates functionalized by tetrathiafulvalene groups: Synthesis, electrochemical studies, and NLO properties. *Inorg. Chem.* **57**, 3742–3752 (2018).

42. Xu, B. & Tao, N. Measurement of Single-Molecule Resistance by Repeated Formation of Molecular Junctions. *Science (80-.).* **301**, 1221–1223 (2003).

43. Kazinczi, R., Szõcs, E., Kálmán, E. & Nagy, P. Novel methods for preparing EC STM tips. *Appl. Phys. A Mater. Sci. Process.* **66**, S535–S538 (1998).

44. Albrecht, T. *et al.* Scanning tunneling spectroscopy in an ionic liquid. *J. Am. Chem. Soc.* **128**, 6574–6575 (2006).

45. Kay, N. J. *et al.* Ionic Liquids As a Medium for STM-Based Single Molecule Conductance Determination: An Exploration Employing Alkanedithiols. *J. Phys. Chem. C* **115**, 21402–21408 (2011).

46. Li, Y. *et al.* Three-State Single-Molecule Naphthalenediimide Switch: Integration of a Pendant Redox Unit for Conductance Tuning. *Angew. Chemie - Int. Ed.* **54**, 13586–13589 (2015).

47. Yan, Y. *et al.* Synthesis and redox-responsive self-assembly of ferrocene grafted Anderson-type polyoxometalate hybrid complexes. *Soft Matter* **8**, 1593–1600 (2012).

48. Kuznetsov, A. M. & Ulstrup, J. Single-molecule electron tunnelling through multiple redox levels with environmental relaxation. *J. Electroanal. Chem.* **564**, 209–222 (2004).

49. Zhang, J. *et al.* Single-molecule electron transfer in electrochemical environments. *Chem. Rev.* **108**, 2737–2791 (2008).

50. Li, Y. *et al.* Transition from stochastic events to deterministic ensemble average in electron transfer reactions revealed by single-molecule conductance measurement. *Proc. Natl. Acad. Sci. U. S. A.* **116**, 3407–3412 (2019).

51. Xiang, L. *et al.* Gate-controlled conductance switching in DNA. *Nat. Commun.* **8**, (2017).